THE JOURNAL OF BIOLOGICAL CHEMISTRY Vol. 278, No. 6, Issue of February 7, pp. 3976–3984, 2003
Printed in U.S.A.

Cell Biology of the Human Thiamine Transporter-1 (hTHTR1)

INTRACELLULAR TRAFFICKING AND MEMBRANE TARGETING MECHANISMS*[S]

Received for publication, October 18, 2002, and in revised form, November 13, 2002
Published, JBC Papers in Press, November 25, 2002, DOI 10.1074/jbc.M210717200

Veedamali S. Subramanian‡§¶, Jonathan S. Marchant¶‖, Ian Parker‖, and Hamid M. Said‡‡§§**

*From the Departments of ‖Neurobiology and Behavior, ‡Medicine, §Physiology and Biophysics, University of California, Irvine, California 92697, the **Department of Pharmacology, University of Minnesota, Minnesota 55455, and the ‡‡Department of Veterans Affairs Medical Center, Long Beach, California 90822*

The human thiamine transporter hTHTR1 is involved in the cellular accumulation of thiamine (vitamin B1) in many tissues. Thiamine deficiency disorders, such as thiamine-responsive megaloblastic anemia (TRMA), which is associated with specific mutations within hTHTR1, likely impairs the functionality and/or intracellular targeting of hTHTR1. Unfortunately, nothing is known about the mechanisms that control the intracellular trafficking or membrane targeting of hTHTR1. To identify molecular determinants involved in hTHTR1 targeting, we generated a series of hTHTR1 truncations fused with the green fluorescent protein and imaged the targeting and trafficking dynamics of each construct in living duodenal epithelial cells. Whereas the full-length fusion protein was functionally expressed at the plasma membrane, analysis of the truncated mutants demonstrated an essential role for both NH_2-terminal sequence and the integrity of the backbone polypeptide for cell surface expression. Most notably, truncation of hTHTR1 within a region where several TRMA truncations are clustered resulted in intracellular retention of the mutant protein. Finally, confocal imaging of the dynamics of intracellular hTHTR1 vesicles revealed a critical role for microtubules, but not microfilaments, in hTHTR1 trafficking. Taken together, these results correlate hTHTR1 structure with cellular expression profile and reveal a critical dependence on hTHTR1 backbone integrity and microtubule-based trafficking processes for functional expression of hTHTR1.

Thiamine (vitamin B1) is a water-soluble micronutrient that is essential for many cellular functions relating to growth and development. For example, thiamine pyrophosphate (the coenzyme form) is important for normal carbohydrate metabolism and energy production (1, 2). Thiamine is not synthesized by humans and other mammals and is obtained from dietary sources via absorption into intestinal epithelia. Deficiencies in cellular thiamine accumulation lead to cardiovascular and neurological disorders and are associated with the inherited condition of thiamine-responsive megaloblastic anemia (TRMA)[1] (1, 3–7). Recent molecular analyses have identified the protein product of the *SLC19A2* gene in humans (chromosome 1q23.3) as the site of mutations that link with TRMA inheritance (2, 7–10). *SLC19A2* encodes a saturable, high affinity human thiamine transporter known as hTHTR1 (2, 7–10), which is expressed in many tissues, including duodenal epithelium (11). The functional properties of hTHTR1 mimic the biochemical characteristics of thiamine uptake in intestinal preparations (reviewed in Refs. 12 and 13). The full-length hTHTR1 protein encodes a 497-amino acid polypeptide with 12 predicted transmembrane-spanning segments and cytoplasmic NH_2- and COOH-terminal regions (2, 8). Several clinically identified mutations have been characterized in hTHTR1 (2, 7–10, 14), including ten prematurely truncated mutants, resulting from either point mutation, deletion, or insertion of nucleotides (reviewed in Refs. 7 and 15). Unfortunately, because nothing is known about the molecular determinants that control the intracellular trafficking and cell surface targeting of hTHTR1, the precise cellular defect of such clinically isolated mutants remains undefined.

Through analogy with other nutrient transporters, the intracellular trafficking and cell surface targeting processes likely involve specific molecular "motifs" within the amino acid sequence of hTHTR1. Such determinants can either be localized within specific regions of the polypeptide or result from protein conformation generated from sequences throughout the entire polypeptide sequence (16, 17). To identify regions of hTHTR1 important for cell surface targeting, we applied confocal imaging techniques to monitor both the steady-state distribution and real-time trafficking of seven hTHTR1 fusion proteins tagged with the enhanced green fluorescent protein (EGFP). We have chosen a human duodenal cell line (HuTu-80) for these studies, because hTHTR1 is expressed at higher levels in human duodenum than other intestinal epithelia (11). Our results show that (i) integrity of both the NH_2-terminal sequence and the transmembrane backbone play an important role in the cell surface expression of hTHTR1; (ii) truncation of the backbone of hTHTR1 between the sixth and seventh transmembrane domains, at a locus where several clinical TRMA mutations cluster (7, 15), results in intracellular retention of hTHTR1; (iii) the cytoplasmic COOH-terminal domain of hTHTR1 is not required for plasma membrane targeting; (iv) the intracellular trafficking dynamics of hTHTR1 are critically dependent on an intact microtubules but not microfilaments. These results highlight how hTHTR1 is delivered to the cell

* This work was supported by the Department of Veterans Affairs, the University of Minnesota Medical School, and Grants DK-56061 and DK-58057 (to H. M. S.), Grant GM-48071 (to I. P.) and National Service Research Award (NRSA) Fellowship Grant F32DK063750-01 (to V. S. S.) from the National Institutes of Health. The costs of publication of this article were defrayed in part by the payment of page charges. This article must therefore be hereby marked "*advertisement*" in accordance with 18 U.S.C. Section 1734 solely to indicate this fact.

[S] The on-line version of this article (available at http://www.jbc.org) contains videos 1–5.

¶ Both authors contributed equally to this work.

§§ To whom correspondence should be addressed. Tel.: 562-826-5811; Fax: 562-826-5731; E-mail: hmsaid@uci.edu.

[1] The abbreviations used are: TRMA, thiamine-responsive megaloblastic anemia; hTHTR1, human thiamine transporter-1; EGFP, enhanced green fluorescent protein; hRFC, human reduced folate carrier; MDCK, Madin-Darby canine kidney cells; RT, reverse transcriptase.

TABLE I

Combination of primers used to prepare the different truncated constructs by PCR

Shown are the sequence and primer combinations used to generate each of the indicated constructs. Restriction sites for *Bam*HI (*boldface*) and *Xho*I (*underlined*) were added to the hTHTR1 primers to assist subcloning into the pEGFP-N3 vector.

Construct	Forward and reverse primers (5′-3′)	Positions	Fragment
		bp	
hTHTR1-EGFP	CCG**CTCGAG**ATGGATGTGCCCGGCC; CGGGATCCTGAAGTGGTTACTTGAGAACT	1–1494	1494
hTHTR1-(1–479)-EGFP	CCG**CTCGAG**ATGGATGTGCCCGGCC; CGGGATCCCATAACACTGACTGCACCACTG	1–1437	1437
hTHTR1-(1–240)-EGFP	CCG**CTCGAG**ATGGATGTGCCCGGCC; CGGGATCCGTCAGTAACAATGCCACCAT	1–721	721
hTHTR1-(1–29)-EGFP	CCG**CTCGAG**ATGGATGTGCCCGGCC; CGGGATCCGCATTCGCGACGGACC	1–87	87
hTHTR1-(241–479)-EGFP	CCG**CTCGAG**ATGACCCCAGCTTCTAACCACCTTC; CGGGATCCCATAACACTGACTGCACCACTG	722–1437	715
hTHTR1-(480–497)-EGFP	CCG**CTCGAG**ATGAAGAAATGTAGAAAGCTGGAAGAT; CGGGATCCTGAAGTGGTTACTTGAGAACT	1438–1494	56
hTHTR1-(30–497)-EGFP	CCG**CTCGAG**ATGTGGTTCTTGCCGACCGC; CGGGATCCTGAAGTGGTTACTTGAGAACT	88–1494	1406
hTHTR1-(19–486)-EGFP	CCG**CTCGAG**ATGCTCCTGCGGACCGCTCG CGGGATCCTTCCAGCTTTCTACATTTCTTCATAAC	55–1458	1403

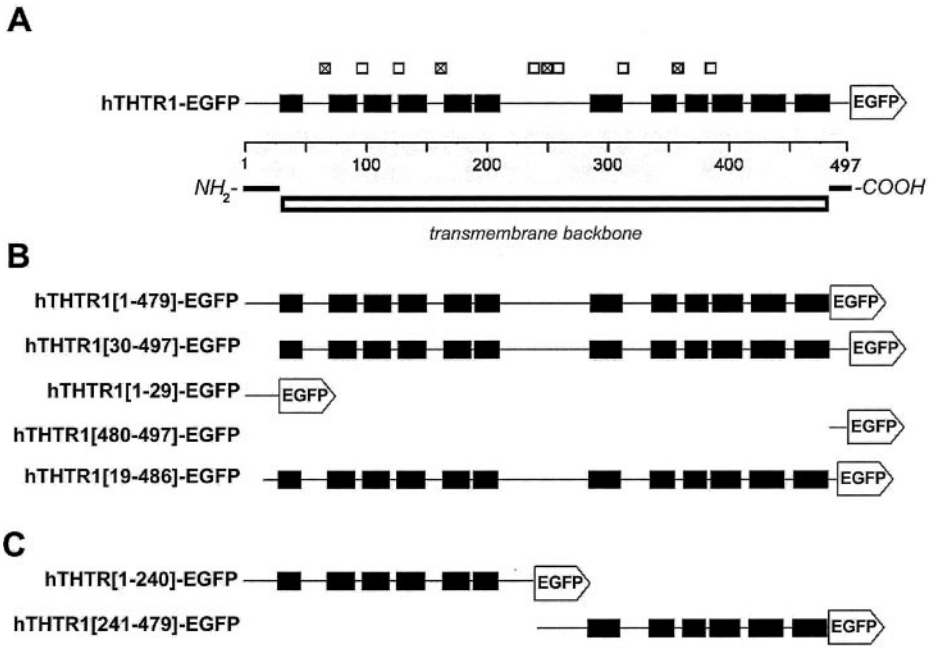

FIG. 1. **Structure of hTHTR1 and construction of fusion proteins.** Schematic representation of hTHTR1-EGFP and seven truncation constructs. In all cases, EGFP was fused to the COOH terminus of the protein. *A*, domain organization of amino acid sequence of hTHTR1-EGFP showing the NH_2-terminal regions (amino acids 1–29); the transmembrane "backbone" (amino acids 30–479) containing 12 transmembrane spanning regions (*black bars*) and the COOH-terminal region (amino acids 480–497). EGFP is illustrated schematically. The positions of ten clinically identified truncation mutants are shown (*open squares*), highlighting the positions of four point mutations (*diagonal crosses*) that result in stop codons, and the lengths of six other prematurely truncated hTHTR1 proteins that result from upstream nucleotide deletion/insertion events. All ten truncation mutants have been identified from clinical presentations of TRMA (see Refs. 7 and 15). *B*, series of five truncation mutants designed to investigate the role of NH_2- and COOH-terminal sequence in hTHTR1 targeting. *C*, two fusion proteins designed to investigate the role of hTHTR1 backbone integrity in cellular targeting.

surface of mammalian epithelia within a physiologically relevant context and define the regions of hTHTR1 in which mutation would likely impair thiamine absorption through disruption of normal cellular targeting mechanisms.

EXPERIMENTAL PROCEDURES

Materials—[^{3}H]Thiamine (specific activity of 555 GBq/mmol) was purchased from ARC (St. Louis, MO). FM4–64 was from Molecular Probes (Eugene, OR). The enhanced green fluorescent protein vector (EGFP-N3) was from BD Biosciences (Palo Alto, CA). Cytochalasin D, nocodazole, colchicine, and γ-lumicolchicine, were from Calbiochem (La Jolla, CA). Antisense oligonucleotides were from Heligen Laboratories (Huntington Beach, CA). G418 was from Life Technologies (Invitrogen, CA). Tissue culture cell lines were obtained from ATCC (Manassas, VA). All other reagents were from Sigma (St. Louis, MO).

Generation of hTHTR1-EGFP and Truncated Constructs—cDNA of the full-length hTHTR1 and truncated constructs were generated by PCR using the primer combinations shown in Table I and conditions specified previously (18, 19). Both the PCR products and the EGFP-N3 vector were digested with the restriction enzymes *Bam*HI and *Xho*I, and the products were gel-isolated and then ligated together to generate in-frame fusion proteins with enhanced green fluorescent protein (EGFP) fused to the COOH terminus of each construct. The nucleotide sequence of each construct was confirmed by sequencing. A schematic representation of each construct is shown below in Fig. 1.

Expression of hTHTR1-EGFP in Xenopus Oocytes—Capped cRNA for oocyte microinjection was synthesized from linearized plasmid DNA using the mMessage mMachine *in vitro* transcription kit (Ambion, Austin, TX). Pigmented oocytes (stages V–VI) were isolated and defolliculated using standard methods (19–21) and then microinjected with either cRNA into the cytoplasm or cDNA into the nucleus. Injected oocytes were separated individually into 96-well plates and maintained in Barth's solution (88 mM NaCl, 1 mM KCl, 2.4 mM $NaHCO_3$, 0.83 mM $MgSO_4$, 0.33 mM $Ca(NO_3)_2$, 0.41 mM $CaCl_2$, 10 mM HEPES, 550 mg/liter sodium pyruvate; 0.05 mg/ml gentamicin, pH 7.4, at 18 °C) with repeated solution changes at least every 18 h. Additional oocytes from the same donor were injected with water as parallel controls for both viability and [^{3}H]thiamine uptake assays. For antisense studies, an equal amount of hTHTR1 cRNA was injected into two batches of oocytes, one batch of which was co-injected with a 5′-cholesterol-modified DNA oligonucleotide (5′-CATCCATCCGGGGCGCGAGGGGAGG) complementary to a sequence upstream of the hTHTR1 start codon (–18 to

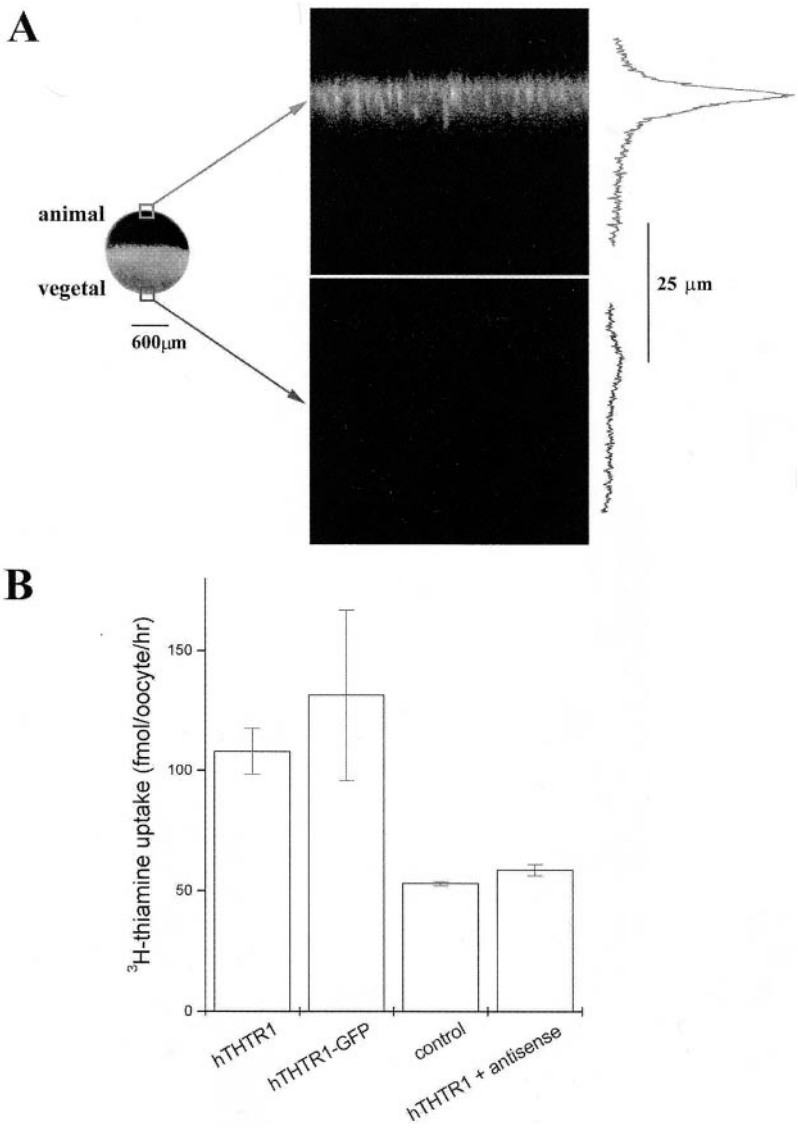

FIG. 2. **Expression of hTHTR1-EGFP in *Xenopus* oocytes.** *A*, bright field image of a pigmented *Xenopus* oocyte (*far left*), to indicate the orientation of the oocyte in the confocal fluorescence images. *Right*, axial (*x-z*) scans into the animal (*top*) and vegetal pole (*bottom*) hemispheres of a *Xenopus* oocyte microinjected 48 h previously with hTHTR1-EGFP cDNA. Images are scaled to the peak fluorescence intensity in the animal hemisphere. Oocytes were injected with hTHTR1-EGFP cDNA to ensure correct processing of the construct through the endogenous oocyte transcription and translation machinery. *Traces* (*far right*) represent fluorescence intensity as a function of depth into the oocyte averaged across a 40-μm section of the laser scan line. *B*, uptake of [^{3}H]thiamine in oocytes injected >48 h previously with hTHTR1 cRNA, hTHTR1-EGFP cDNA, water, or hTHTR1 cRNA and an antisense oligonucleotide. Results represent the mean ± S.E. from three different donor animals.

+7 base pairs). [^{3}H]Thiamine uptake experiments were performed at least 48 h after injection by incubating six to eight oocytes for 1 h at room temperature in Barth's solution (200 μl) supplemented with 150 nM [^{3}H]thiamine. Uptake was terminated by several washes in ice-cold Barth's solution (5 ml), after which individual oocytes were transferred to scintillation vials and dissolved in 10% SDS (250 μl) before scintillation counting.

Cell Culture and Transient Transfection—Human duodenal-derived intestinal epithelial cells (HuTu-80), opossum kidney cells (OK), human embryonic kidney cells (HEK-293), human hepatoma cells (HepG2), and Madin-Darby canine kidney cells (MDCK) were maintained in minimal essential medium, supplemented with 10% fetal bovine serum, glutamine (0.29 g/liter), sodium bicarbonate (2.2 g/liter), penicillin (100,000 units/liter), and streptomycin (10 mg/liter). For transient transfection, cells were grown on sterile glass-bottomed Petri dishes (MatTek, MA) and transfected at 90% confluency with 1 μg of plasmid DNA using LipofectAMINE 2000 (Invitrogen, CA). After 24 h, cells were analyzed by confocal microscopy.

Generation of Stable Cell Lines—Three stable cell lines were generated by selection of hTHTR1-EGFP, hTHTR1-pcDNA3.1, and EGFP-N3 expressing HuTu-80 cells with G418 (0.8 mg/ml) in minimal essential medium supplemented with 10% fetal bovine serum. Molecular analyses of stable cell lines were performed using semi-quantitative RT-PCR. Total RNA (5 μg) was isolated from stably transfected and untransfected HuTu-80 cells and used to generate first-stranded cDNA with hTHRT1 gene-specific primers (Table I) and a superscript First-Strand synthesis kit (22). After subsequent PCR reactions, agarose gels (0.7%) were stained with ethidium bromide, and the intensity of the product band was quantified by densitometry. For [^{3}H]thiamine uptake experiments, cell monolayers were incubated for 3 min at 37 °C in Krebs-Ringer buffer (pH 7.4) supplemented with [^{3}H]thiamine (30 nM). Uptake was terminated by addition of ice-cold Krebs-Ringer buffer, and accumulated radioactivity was measured by scintillation counting.

Confocal Microscopy—Cells were imaged using either a customized laser scan confocal microscope (23) or a video-rate scanning confocal microscope (24). Both microscopes were based on an Olympus IX70 inverted microscope fitted with a 40× oil-immersion objective. Fluorophores were excited using the 488-nm line from an argon ion-laser, and emitted fluorescence was monitored with a 530 ± 20-nm band pass (EGFP) or a 650-nm long-pass filter (FM4–64). Using the linescan microscope (Figs. 2*A*, 3, 4, and 5*A*), frame scans were obtained by scanning the laser line either laterally (*x-y* scan) or axially (*x-z* scan) within the cell. For real-time images of vesicular trafficking, hTHTR1-EGFP fluorescence was monitored using the video-rate confocal microscope (Figs. 6 and 7). Petri dishes were maintained at 22 °C or 37 °C using a thermostatted stage mount. Images were captured at 30 Hz over a 40-μm square region using a video-acquisition board/frame grabber and archived onto digital tape. For image processing, video data were digitized into image stacks using the stream acquisition function of the Metamorph imaging package (Universal Imaging, Downingtown, PA). Raw data stacks were averaged (as merges of two sequential 33-ms frames) and low pass-filtered before analysis. Frame-to-frame particle tracking was performed using customized macro routines in Metamorph to generate two-dimension (*x-y*) tracks of discrete particles over time. From such plots, quantitative data concerning the linear velocities and associated vectorality of individual structures could be analyzed throughout the entire recording period. Quick-time movies of video sequences are appended as supplementary material (videos 1–5).

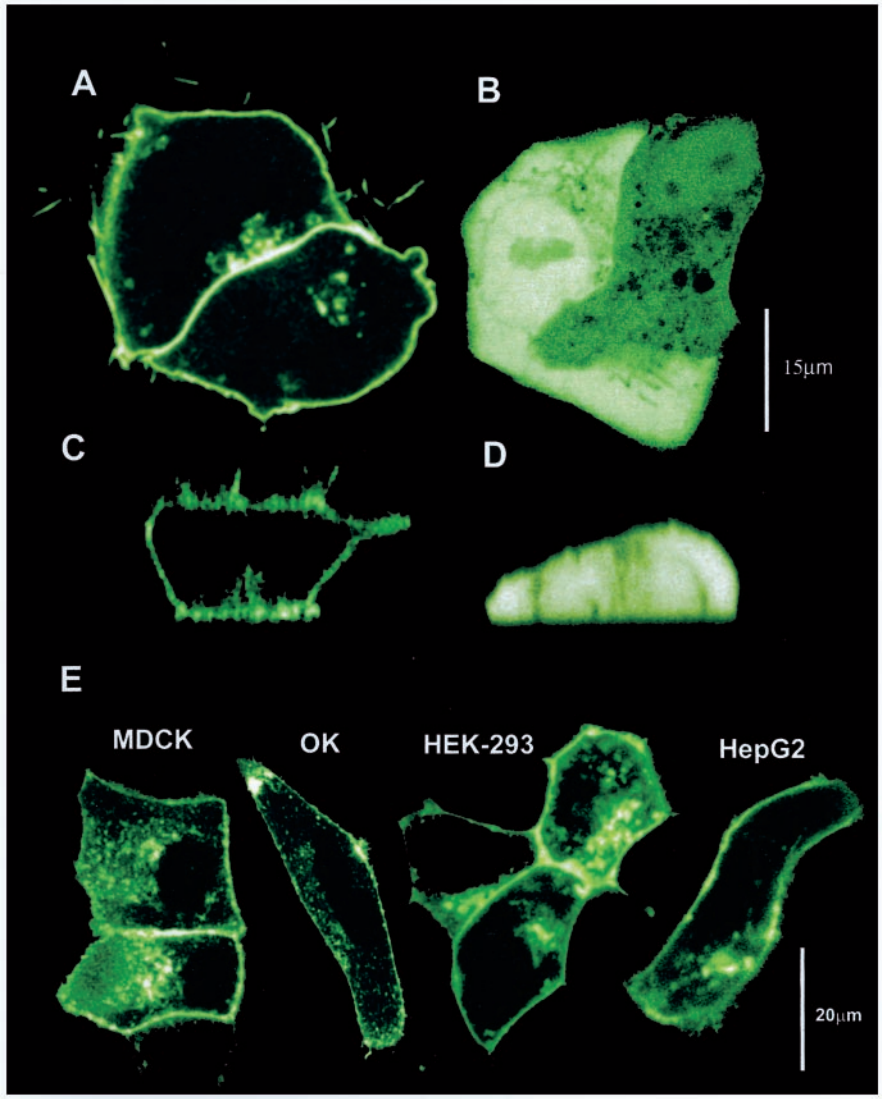

FIG. 3. **Distribution of hTHTR1-EGFP in epithelial cells.** *A* and *B*, lateral *x-y* confocal images of HuTu-80 cells transiently transfected with hTHTR1-EGFP (*A*) or pEGFP alone (*B*). *C* and *D*, axial confocal sections (*x-z*) of HuTu-80 cells expressing hTHTR1-EGFP (*C*) or EGFP alone (*D*). *E*, lateral confocal images showing expression of hTHTR1-EGFP in the cell membrane of MDCK (canine kidney), OK (opossum kidney), HepG2 (human hepatoma), and HEK-293 (human embryonic kidney) cell lines.

RESULTS

Design of hTHTR1 Truncations—The schematic representation of the full-length hTHTR1-EGFP fusion protein in Fig. 1*A* illustrates the structural organization of the protein, comprising an NH_2-terminal cytoplasmic region (amino acid residues 1–29), a transmembrane domain with 12 predicted transmembrane-spanning regions (amino acid residues 30–479), and a COOH-terminal cytoplasmic domain (amino acid residues 480–497) that was fused to EGFP. To identify regions important for cell surface expression, we generated a series of seven truncated fusion proteins (Fig. 1, *B* and *C*). First, we analyzed the role of NH_2-terminal, transmembrane backbone, and COOH-terminal regions in hTHTR1 targeting (Fig. 1*B*). Second, we examined the effect of premature truncation between the sixth and seventh transmembrane domains of hTHTR1 (Fig. 1*C*), where three premature truncations (amino acid residues 239, 250, and 259) occur in clinical presentations of TRMA (7, 15).

Functionality of the hTHTR1-EGFP—We first confirmed the functionality and appropriate cellular targeting of the full-length hTHTR1-EGFP fusion construct by expressing the protein in *Xenopus* oocytes following nuclear injection of cDNA encoding hTHTR1-EGFP (Fig. 1*A*). Two days after microinjection, oocytes were imaged by confocal microscopy for hTHTR1-EGFP expression. In all oocytes examined (n = 8 cells), hTHTR1-EGFP fluorescence was evident with an average 11.0 ± 2.5-fold greater peak fluorescence in the animal compared with the vegetal pole (Fig. 2*A*). Fluorescence was confined to a radial band 5.2 ± 1.4 μm wide, consistent with the thickness of the invaginated oocyte plasma membrane (19). To confirm localization of hTHTR1-EGFP to the cell surface, and to compare the functionality of hTHTR1-EGFP relative to hTHTR1, we measured [^{3}H]thiamine uptake in *Xenopus* oocytes heterologously expressing either construct. Oocytes expressing hTHTR1 or hTHTR1-EGFP exhibited [^{3}H]thiamine accumulation (108.0 ± 9.6 and 131.5 ± 35.5 fmol/oocyte/h, respectively) that was about double that in water-injected controls (53.0 ± 1.0 fmol/oocyte/h) or oocytes co-injected with hTHTR1 cRNA and an antisense oligonucleotide to prevent translation of hTHTR1 (58.6 ± 2.4 fmol/oocyte/h). These values for [^{3}H]thiamine uptake in cells expressing hTHTR1-EGFP (~1.5-fold uptake) were similar to those reported elsewhere on expression of hTHTR1 cDNA (2, 14). Thus, the functionality of the hTHTR1-EGFP fusion protein was not impaired by COOH-terminal fusion to GFP, and the fusion protein correctly targeted to the cell surface.

Plasma Membrane Localization of hTHTR1-EGFP in Epithelial Cell Lines—To study the targeting of hTHTR1-EGFP in mammalian epithelia, cDNA encoding hTHTR1-EGFP was transiently transfected into a variety of epithelial cell lines, and the resulting fluorescence distribution was analyzed by confocal microscopy. In HuTu-80 cells, hTHTR1-EGFP expres-

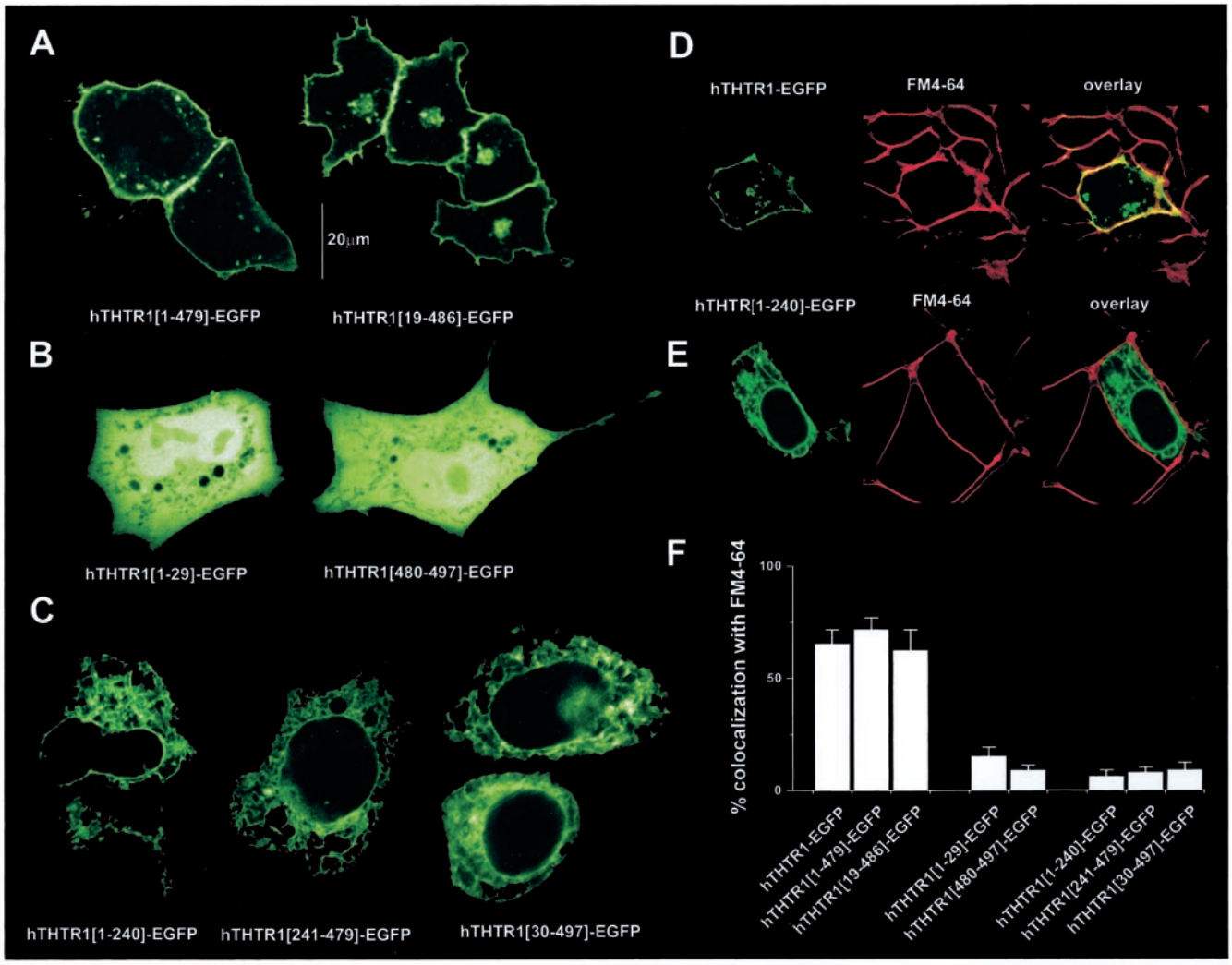

FIG. 4. **Cellular distribution of truncated hTHTR1-EGFP constructs in HuTu-80 cells.** HuTu-80 cells were transiently transfected with cDNA encoding the indicated mutants and lateral (*x-y*) confocal images were obtained 48 h later. The laser power was individually adjusted to obtain final images of equivalent brightness, and differences in intensity do not, therefore, reflect differences in protein expression between particular constructs. Constructs are grouped into categories (*A–C*) as detailed in the results. *D* and *E*, images of HuTu-80 cells stained with FM4–64 that were previously transfected with hTHTR1-EGFP (*D*) and hTHTR1-(1–240)-EGFP (*E*) to show *green fluorescence* of EGFP alone (*left*), *red fluorescence* of FM4–64 in the plasma membrane (*middle*), and a dual channel overlay (*right*). *F*, bar graph showing percentage co-localization of EGFP with FM4–64 fluorescence for each indicated hTHTR1 construct. Data are from $n > 10$ transfected cells.

sion was evident in the cell membrane as well as in processes extending from the cell surface and a variety of intracellular structures (Fig. 3*A*). This distribution differed markedly from HuTu-80 cells transfected with EGFP alone, in which the entire cytoplasmic volume was fluorescence (Fig. 3*B*). These contrasting distributions were also apparent in axial scans (*side views*) of HuTu-80 cells expressing either hTHTR1-EGFP or EGFP alone (Fig. 3, *C* and *D*, respectively). A similar plasma membrane targeting of hTHTR1-EGFP was also apparent in several other cell lines, including MDCK, OK, HEK-293, and HepG2 (Fig. 3*E*).

Determination of Regions of hTHTR1 Important for Cell Surface Targeting—To investigate the role of specific regions of hTHTR1 structure in cell surface targeting, we constructed a series of hTHTR1 truncations (Fig. 1, *B* and *C*) and compared their expression profile with the full-length hTHTR1-EGFP fusion protein. Fig. 4 (*A–C*) shows representative confocal images (*x-y* scans) of HuTu-80 cells imaged 48 h after transient transfection with each construct. Several expression patterns were apparent, which could be grouped into three classes: 1) expression predominantly at the cell surface (hTHTR1-(1–479)-EGFP and hTHTR1-(19–486), Fig. 4*A*); 2) a cytosolic, non-membrane-bound expression (hTHTR1-(1–29)-EGFP and hTHTR1-(480–497)-EGFP, Fig. 4*B*), and 3) expression confined within intracellular membranes (hTHTR1-(1–240)-EGFP, hTHTR1-(241–479)-EGFP, and hTHTR-(30–497)-EGFP, Fig. 4*C*).

Targeting of different hTHTR1-EGFP constructs to the cell surface was quantified utilizing a distribution overlap assay (18, 25), in which cells transfected with individual hTHTR1-EGFP fusion constructs were co-stained by extracellular application of the *red* lipophilic marker FM4–64 to selectively stain the plasma membrane. Fig. 4 illustrates this method for cells expressing hTHTR1-EGFP (Fig. 4*D*) and hTHTR1-(1–240)-EGFP (Fig. 4*E*). The green fluorescence of hTHTR1-EGFP overlapped considerably with the *red* fluorescence of FM4–64 to yield a *yellow color* indicating a high degree of localization of hTHTR1-EGFP at the cell surface (Fig. 4*D*). In contrast, little fluorescence co-localization was observed with hTHTR1-(1–240)-EGFP (Fig. 4*E*), which remained localized within intracellular membranes. Fig. 4*F* shows collated measurements of fluorescence co-localization obtained by this method for hTHTR1-EGFP and all seven truncated constructs. A high degree (~60%) of fluorescence overlap was observed in cells

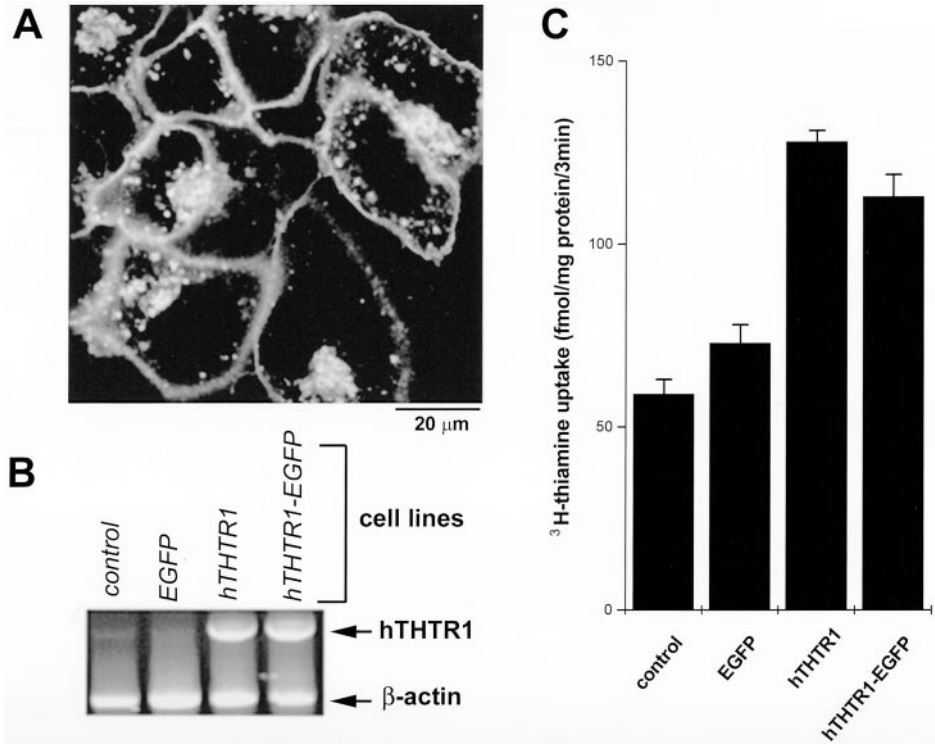

FIG. 5. **Properties of a HuTu-80 cell line stably transfected with hTHTR1-EGFP.** *A*, confocal linescan image (*x-y*) of hTHTR1-EGFP distribution in a HuTu-80 cell line maintained for 8 weeks under G418 antibiotic selection. *B*, RT-PCR detection of hTHTR1 mRNA from untransfected (control), as well as three different HuTu-80 stable cell lines. *C*, [^{3}H]thiamine uptake assays in mock transfected and stably transfected HuTu-80 cell lines. Results represent the mean ± S.E. from $n = 3$ experiments.

expressing hTHTR1-EGFP, hTHTR1-(1–479)-EGFP, and hTHTR1-(19–486)-EGFP, confirming that each of these constructs targeted to the cell surface. Little co-localization (~10%) was seen with the remaining constructs confirming their inability to reach the plasma membrane.

Establishment of a Stable HuTu-80 Cell Line for Analysis of hTHTR1-EGFP Trafficking—To facilitate investigation of the role of the cytoskeleton in controlling the delivery to hTHTR1-EGFP to the cell surface, we generated a stably expressing HuTu-80 cell line. Fig. 5*A* shows a confocal image of a HuTu-80 monolayer after 8 weeks of antibiotic selection, when the majority of cells (~60%) exhibited the characteristic cell surface and intracellular distribution of hTHTR1-EGFP. Two further stable cell lines, expressing either hTHTR1 or EGFP alone, were established in parallel as controls. RT-PCR analysis of all three stable cell lines showed that hTHTR1 mRNA expression was ~5-fold greater in both the hTHTR1 and hTHTR1-EGFP stable HuTu-80 clones compared with the EGFP-expressing stable cell line or mock transfected HuTu-80 cells (Fig. 5*B*). Furthermore, uptake of [^{3}H]thiamine in both the hTHTR1-EGFP (113 ± 6 fmol/mg of protein/3 min) and hTHTR1 (128 ± 3 fmol/mg of protein/3 min) stable cell lines was significantly greater than in the EGFP stable cell line (73 ± 5 fmol/mg of protein/3 min) or in untransfected HuTu-80 cells (59 ± 4 fmol/mg of protein/3 min). Taken together, these data further support the functionality of the hTHTR1-EGFP fusion construct and establish the validity of this stable cell line for analyses of hTHTR1-EGFP properties.

Intracellular Trafficking Dynamics of hTHTR1—Confocal imaging of the stable hTHTR1 HuTu-80 cell line revealed numerous vesicular-like structures within the cytoplasm (Figs. 5*A* and 6*A*). The dimensions of these structures ranged between 0.5 and 1.5 μm (Fig. 6*B*), suggesting that hTHTR1-EGFP localized within a heterogeneous population of intracellular vesicles. Vesicles were evident throughout the cytoplasm, but fluorescence was most concentrated close to the nucleus, which presumably represents the initial sites of hTHTR1-EGFP biosynthesis (see "Discussion"). To investigate the dynamics of individual vesicles trafficking toward the cell surface, we employed video-rate confocal imaging to capture image sequences with sufficient temporal resolution (30 frames per second) to track the movement of single vesicles in real time. An analysis of the video data (supplementary video 1), illustrated by a single image frame in Fig. 6*A*, is shown schematically in Fig. 6*C*. The coordinates of fluorescent vesicles were tracked at 66-ms intervals (two-frame averages) to generate color-coded tracks depicting their motion. Several tracks are shown expanded in Fig. 6*C* and illustrate three generalized features of hTHTR1-EGFP dynamics.

First, in any given cell, the population of hTHTR1-EGFP-containing vesicles exhibited a wide variation in motility, some vesicles remained predominantly static (*e.g.* vesicle *iv*, Fig. 6*C*), whereas others were highly dynamic (*e.g.* vesicles *i*, *ii*, and *iii*, Fig. 6*C*). The distribution between the "dynamic" and "static" phenotype was temperature-dependent, with progressively more vesicles becoming motionless at lower temperature (data not shown). Furthermore, the velocity of vesicular movements increased with temperature. At 22 °C, the average vesicular velocity (including stationary periods) was 0.43 ± 0.13 μm s^{-1} ($n = 25$ vesicles), compared with 0.92 ± 0.21 μm s^{-1} at 37 °C ($n = 93$ vesicles).

Second, the high temporal resolution of the video-rate confocal records revealed two discrete components to the dynamics of individual vesicles, namely periods of rapid, approximately linear motion (*e.g.* black lines, vesicle *iii*, Fig. 6*C*) interspersed with periods of relatively immobility during which vesicles displayed small Brownian-like movements (*e.g.* arrow, vesicle *iii*, Fig. 6*C*). Because of this "stop-start" behavior, "average velocity" measurements presented above underestimate the peak velocity of hTHTR1-EGFP-containing vesicles. Therefore, we quantified velocities during the periods of rapid, directed linear movements (Fig. 6*D*). At 37 °C the average linear velocity was 1.71 ± 0.13 μm/s, decreasing to 0.73 ± 0.36 μm/s at 22 °C ($n = 38$ vesicles, 5 cells). However, at both temperatures the "run length" (the length of linear segments) was similar, 2.75 ± 0.22 μm at 22 °C and 3.22 ± 0.22 μm at 37 °C.

Third, the movement of vesicles was strikingly multidirectional. Rather than displaying a consistent progression toward

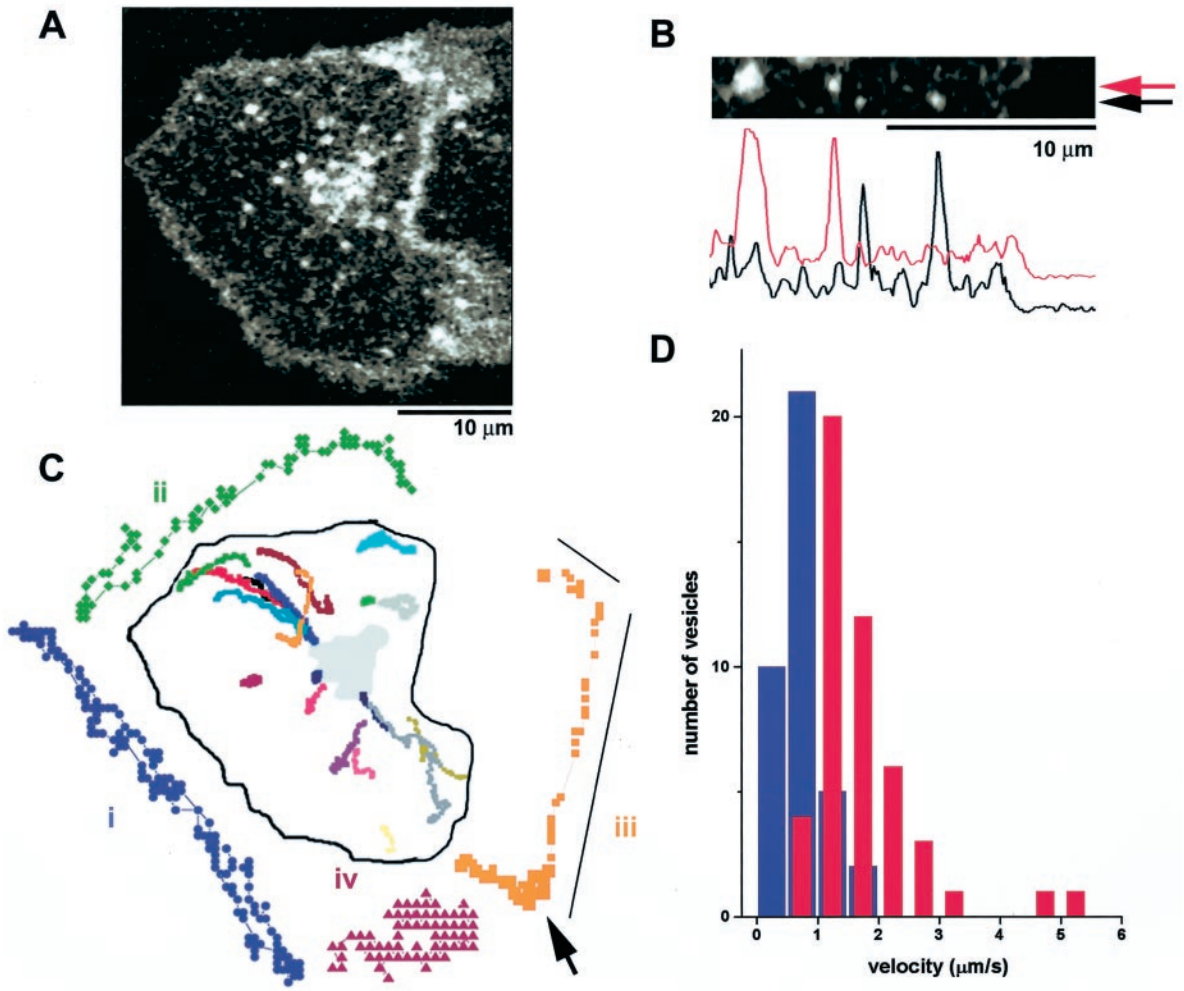

FIG. 6. **Vesicular trafficking of hTHTR1-EGFP in a stable HuTu-80 cell line.** *A*, a single frame from a video-rate confocal image showing the distribution of hTHTR1-EGFP-containing vesicles in a stably transfected HuTu-80 cell at 37 °C. The entire video sequence is appended as supplementary video material (video 1). *B*, dimensions of hTHTR1-EGFP-containing vesicular structures in the cytoplasm of a stably transfected HuTu-80 cell. Fluorescence profiles of four vesicles are measured along 3-pixel wide lines at the *red* and *black arrows*. *C*, tracks of individual vesicle movements schematically represented from the cell shown in *A*. For clarity, only a fraction of the total vesicular tracks are displayed. The high density of vesicles near the center of the cell (indicated by *gray shading*) made it impossible to identify discrete structures within this region. Individual tracks (*i* through *iv*) have been expanded to provide examples of (*i*) a vesicle exhibiting bi-directional movements, (*ii*) a vesicle tracking beneath the cell surface, (*iii*) a vesicle showing rapid linear movements interspersed by periods of relative immobility, and (*iv*) a static vesicle. *D*, histograms showing distribution of vesicular velocities quantified at 22 °C (*blue*) and 37 °C (*red*) during periods of linear movements.

the cell surface from the interior of the cell, vesicles frequently retracted their steps (*e.g.* vesicle *i*, Fig. 6*C*). Similar behavior was also apparent when vesicles were in close proximity to the cell boundary, where they appeared to track cirumferentially beneath the plasma membrane (*e.g.* vesicle *ii*, Fig. 6*C*). Despite the multidirectional nature of vesicular motion, vesicles moving through the same area of the cytoplasm showed significant overlap in their tracks (Fig. 6*C*).

Role of Microtubules and Actin Microfilaments in hTHTR1-EGFP Trafficking—Having quantified the characteristics of vesicular motion at 37 °C (Fig. 6*D*), we proceeded to examine the effect of cytoskeletal disruption on the motion of individual hTHTR1-EGFP-containing vesicles. Image sequences were recorded before and after addition of either the microtubule disrupting drugs nocodazole or colchicine (with γ-lumicolchicine as a negative control) or the microfilament disrupting drug cytochalasin D.

Fig. 7 shows the effect of incubation of HuTu-80 cells with nocodazole (Fig. 7*A*, 10 μM for 5 min), colchicine (Fig. 7*B*, 10 μM for 15 min), γ-lumicolchicine (Fig. 7*C*, 50 μM for 30 min), or cytochalasin D (Fig. 7*D*, 10 μM for 30 min), together with the measurements of the effects of each compound on the linear velocities of hTHTR1-EGFP motion at various times after drug addition (Fig. 7*E*). Each diagram of vesicular motion (Fig. 7, *A–D*) is associated with a supplementary video (videos 2–5 in supplemental material) from which the tracking data were derived. Incubation of cells with nocodazole rapidly inhibited the linear motion of hTHTR1-EGFP-containing vesicles within 5 min (Fig. 7, *A* and *E*). Colchicine exhibited a similar effect albeit over a slower time course, with maximal inhibition taking up to 15 min (Fig. 7, *B* and *E*). In contrast, addition of γ-lumicolchicine (50 μM) failed to impede vesicular motion, even with incubation periods as long as 30 min (Fig. 7, *C* and *E*). Similarly, cytochalasin D had little effect on the linear motions of hTHTR1-containing vesicles (Fig. 7, *D* and *E*).

DISCUSSION

In this study, we investigated the physiological behavior of hTHTR1 within intestinal epithelial cell lines with regard to three issues. First, what regions of the hTHTR1 polypeptide are important for targeting hTHTR1 to the cell surface? Second, how do clinically relevant hTHTR1 truncations affect the cellular targeting of hTHTR1? Third, what cytoskeletal elements mediate hTHTR1 trafficking? To resolve these ques-

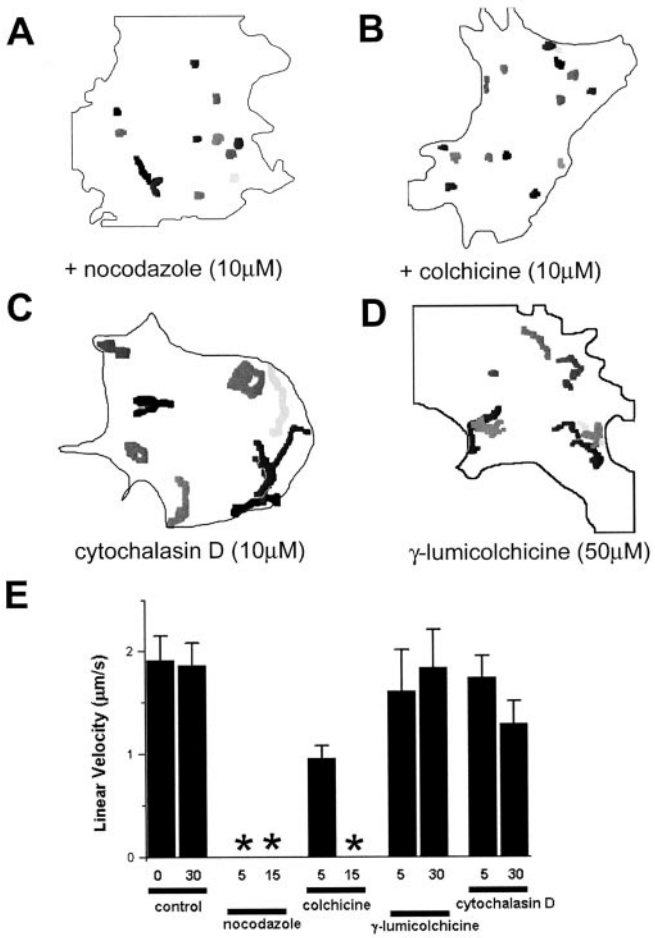

FIG. 7. **Effect of cytoskeletal disruption on the movement of hTHTR1-EGFP-containing vesicles.** Schematic representations of vesicular dynamics in HuTu-80 cells stably transfected with hTHTR1-EGFP treated with: *A*, nocodazole (10 μM, 5 min); *B*, colchicine (10 μM, 15 min); *C*, cytochalasin D (10 μM, 30 min); *D*, γ-lumicolchicine (50 μM, 30 min). Each image is associated with a video file attached as supplementary material (videos 2–5). *E*, histogram showing the effect of pharmacological treatments on the observed linear velocities of hTHTR1-EGFP-containing vesicles. Durations of incubation with each drug concentration are shown numerically on the *x-axis*. *Asterisks* indicate an inability to measure linear velocities owing to no observed motion. Data are from $n \geq 5$ cells.

tions, we employed confocal microscopy to image the dynamics of hTHTR1-EGFP fusion proteins. This strategy has proved a powerful approach to monitor the targeting and expression of nutrient transporters and other proteins, because it allows localization with high spatial and temporal resolution in live cells (18, 25, 26). Heterologous expression of hTHTR1-EGFP in either mammalian epithelial cell lines (Figs. 3 and 5*A*) or the *Xenopus* oocyte expression system (Fig. 2*A*), resulted predominantly in expression of hTHTR1-EGFP fluorescence at the cell surface, as expected for a transporter protein, as well as in cellular processes extending from the plasma membrane and a variety of intracellular structures (see below). Ligation of EGFP to the COOH terminus of hTHTR1 did not impair functionality, as assessed by [^{3}H]thiamine accumulation in both *Xenopus* oocytes (Fig. 2*B*), and a stably expressing human duodenal cell line (Fig. 5*C*).

Regions of hTHTR1 Important for Cellular Targeting—The delivery of proteins to specific cellular compartments depends on the presence of targeting commands embedded as primary sequence, structural conformations, or post-translational processing signals within the protein structure (27, 28). Many "motifs" responsible for directing nutrient transporters to the plasma membrane of epithelial cells have been localized within the NH_2 terminus (29), COOH terminus (30), and/or the transmembrane backbone regions of individual proteins (18). Here we show that *both* NH_2-terminal sequence (within amino acids 19–29) as well as determinants within the transmembrane backbone are important in directing the expression and consequent export of hTHTR1 from the endoplasmic reticulum to the plasma membrane. This conclusion is based on the following evidence. First, the COOH-terminal cytoplasmic region (amino acids 480–497) was unimportant for plasma membrane targeting, because removal of this region failed to prevent cell surface localization (hTHTR1-(1–479)-EGFP). In contrast, removal of the NH_2-terminal sequence (amino acids 1–29) prevented cell surface expression of the truncated protein (hTHTR1-(30–497)-EGFP), which was retained within intracellular membranes (Fig. 4*C*). Second, the NH_2-terminal sequence alone was not sufficient for cell surface expression, because hTHTR1-(1–240)-EGFP, a construct in which the entire NH_2-terminal sequence was preserved, but the polypeptide backbone was truncated after six transmembrane helices, was retained within intracellular membranes. The role of the polypeptide backbone was underscored by the observation that hTHTR1-(19–486) in which both the NH_2- and COOH-terminal regions were partially truncated, but the integrity of the transmembrane domains preserved, was targeted to the cell surface (Fig. 4, *A* and *F*). Further experiments are needed to delimit whether polypeptide backbone integrity *per se*, or specific determinants downstream of the truncation site, are needed for plasma membrane expression. The important point is that, if COOH determinants exist, they do not function in isolation, because hTHTR1-(241–479) was also defective at export from intracellular membranes. Most likely, plasma membrane targeting is dependent on both NH_2-terminal sequence and determinants distributed throughout the hTHTR1 polypeptide backbone.

A final important point relates to our knowledge of targeting determinants in other members of the *SLC19A* gene family. As the protein product of the *SLC19A2* gene, hTHTR1 shares significant sequence identity (~40% (2, 8)) with the human reduced folate carrier (hRFC), the protein product of the *SLC19A1* gene (31). Topological analysis of both proteins suggests a similar 12 transmembrane-spanning topology (Refs. 2, 32, and 33, but see Ref. 10). We recently analyzed the effect of specific domain ablations on hRFC targeting (18, 19) and demonstrated that polypeptide backbone integrity plays a crucial role in the plasma membrane expression of hRFC. This result mimics that observed here with hTHTR1, in that the polypeptide backbone of either transporter (hTHTR1-(19–486)-EGFP or hRFC-(19–466)-EGFP) with minimal flanking sequence is sufficient to direct cell surface expression. One subtle difference with hTHTR-1 is that the NH_2-terminal sequence (amino acids 19–29) is more critical for cell surface expression than the corresponding region in hRFC (18). This may relate to the difference in net positive charge of the NH_2-terminal domain of hTHTR1 ("+4") compared with hRFC ("0"), which may be crucial in directing appropriate protein translocation and folding within the endoplasmic reticulum membranes (34). Overall these results suggest the possible conservation of targeting mechanisms between these closely related cousins within the major facilitator superfamily of transporters (35). It remains to be seen whether this homology extends to hTHTR2, the protein product of the recently characterized *SLC19A3* gene (36, 37), which encodes a second human thiamine transporter with even greater amino acid residue identity to hTHTR1 (~48% (36, 37)).

Clinical Relevance of Truncations within the hTHTR1 Polypeptide Backbone—TRMA is a rare autosomal recessive

disorder, attributed to mutational impairment of hTHTR1 function caused by specific mutations in the *SLC19A2* gene (2, 7–10, 14, 15). At least fourteen distinct mutations have been identified from TRMA patients (7, 15) of which 10 result in premature truncation of hTHTR1 (Fig. 1*A*). Three of these truncations (239, 250, and 259 amino acids (8)) result in premature termination within a region normally between the sixth and seventh transmembrane helices (10). Confocal imaging of hTHTR1-(1–240)-EGFP showed that the truncated protein is retained within intracellular membranes (Fig. 4*C*), with no visible cell surface expression (Fig. 4*E*). Therefore, the three clinically relevant truncations occurring within this same region likely result in abrogation of cell surface expression. Because the four upstream truncations (after amino acids 66, 97, 127, and 162) lack further amino acids (Refs. 7, 8, 10, and 15), each of these truncations likely results in intracellular retention of the protein product. Further experiments are needed to identify the cellular localization of the three remaining clinically identified truncations (313, 358, and 385 amino acids in length) (Refs. 9, 15, and 38), although we note that similar sized truncations of hRFC backbone resulted in intracellular retention (18).

Intracellular Trafficking of hTHTR1-EGFP—Generation of a stable hTHTR1-EGFP-expressing duodenal cell line facilitated analysis of hTHTR1-EGFP trafficking as synthesis of hTHTR1-EGFP was ongoing and the population of intracellular fluorescent structures more numerous than with transient transfection. The steady-state distribution of hTHTR1-EGFP was defined by a strong cell surface expression, together with considerable fluorescence within a juxtanuclear pool, most likely the Golgi apparatus. Vesicular motility was critically dependent on an intact microtubular cytoskeleton, as shown by the effects of pharmacological disruption with nocodazole or colchicine, but not γ-lumicolchicine as a negative control (Fig. 7). Furthermore, video-rate confocal measurements of vesicular dynamics (Fig. 6, average moving velocities of ~1.7 μm/s and run lengths of ~3 μm) are consistent with microtubule-based transport of different cargos in other cell types (39, 40), as well as speeds of microtubule-based motors measured *in vitro* (41). A striking result was the observation of multidirectional vesicular motion, both toward and away from the cell surface, as well as circumferential movements beneath the plasma membrane (Fig. 6). These images suggest that the trafficking and insertion of hTHTR1 into the plasma membrane may be physiologically regulated events, and we are currently investigating mechanisms that may influence the *net* progression of hTHTR1 transporters toward, and removal from, the cell surface.

Summary—These studies show that, unlike many nutrient transporters, the molecular determinants that dictate hTHTR1 targeting to the cell surface are not located within the COOH-terminal cytoplasmic tail of the polypeptide but are dependent on residues within both the NH_2-terminal region and the polypeptide backbone. Premature truncation of the polypeptide backbone, as seen in several independent clinical mutations in hTHTR1, causes intracellular retention of the protein. Finally, trafficking of hTHTR1 to the cell surface is critically dependent on intact microtubules but not microfilaments.

Acknowledgment—We thank Arsalan Hejazi for help with data analysis.

REFERENCES

1. Berdanier, C. D. (1998) *Advanced Nutrition Micronutrients*, pp. 80–88, CRC, New York
2. Dutta, B., Huang, W., Molero, M., Kekuda, R., Leibach, F. H., Devoe, L. D., Ganapathy, V., and Prasad, P. D. (1999) *J. Biol. Chem.* **274,** 31925–31929
3. Tanphaichirt, V. (1994) *Modern Nutrition in Health and Disease*, pp. 359–375, Lea and Febiger, New York
4. Victor, M., and Adams, R. D. C. G. H. (1989) *The Wernicke-Korsakoff Syndrome and Related Neurological Disorders Due to Alcoholism and Malnutrition*, Davis, Philadelphia
5. Mandel, H., Berant, M., Hazani, A., and Naveh, Y. (1984) *N. Engl. J. Med.* **311,** 836–838
6. Rogers, L. E., Porter, F. S., and Sidbury. J. B. (1969) *J. Pediatr.* **74,** 494–504
7. Raz, T., Labay, V., Baron. D., Szargel, R., anbinder, Y., Barrett, T., Rabl, W., Viana, M. B., Mandel, H., Baruchel, A., Cayuela, J. M., and Cohen, N. (2000) *Hum. Mutat.* **13,** 37–42
8. Diaz, G. A., Banikazemi, M., Oishi, K., Desnick, R. J., and Gelb, B. D. (1999) *Nat. Genet.* **22,** 309–312
9. Fleming, J. C., Tartaglini, E., Steinkamp, M., Schorderit, D. F., Cohen, N., and Neufeld, E. J. (1999) *Nat. Genet.* **22,** 305–308
10. Labay, V., Raz, T., Baron, D., Mandel, H., Williams, H., Barrett, T., Szargel, R., McDonald, L., Shalata, A., Nosaka, K., Gregory, S., and Cohen, N. (1999) *Nat. Genet.* **22,** 300–304
11. Reidling, J. C., Subramanian, V. S., Dudeja, P. K., and Said, H. M. (2002) *Biochim. Biophys. Acta* **1561,** 180–187
12. Rindi, G., and Laforenza, U. (2000) *Proc. Soc. Exp. Biol. Med.* **224,** 246–255
13. Said, H. M., Rose, R., and Seetharam, B. (2000) in *Intestinal Absorption of Water-soluble Vitamins: Cellular and Molecular Aspects* (Barrett, K. E., and Donowitz, M., eds) pp. 37–75, Academic Press, San Diego
14. Balamurugan, K., and Said, H. M. (2002) *Am. J. Physiol.* **283,** G37–G43
15. Neufield, E. J., Fleming, J. C., Tartaglini, E., and Steinkamp, M. P. (2001) *Blood Cells Mol. Dis.* **27,** 135–138
16. Ikonen, E., and Simons, K. (1998) *Semin. Cell. Dev. Biol.* **9,** 503–509
17. Lalioti, V., Vergarajauregui, S., and Sandoval, I. V. (2001) *Mol. Membr. Biol.* **18,** 257–264
18. Marchant, J. S., Subramanian, V. S., Parker, I., and Said, H. M. (2002) *J. Biol. Chem.* **277,** 33325–33333
19. Subramanian, V. S., Marchant, J. S., Parker, I., and Said, H. M. (2001) *Am. J. Physiol.* **281,** G1477–G1486
20. Marchant, J. S., and Parker, I. (2001) *Br. J. Pharmacol.* **132,** 1396–1410
21. Kumar, C. K., Nguyen, T. T., Gonzales, F. B., and Said, H. M. (1998) *Am. J. Physiol.* **274,** C289–C294
22. Said, H. M., Ortiz, A., Subramanian, V. S., Neufield, E. J., Moyer, M. P., and Dudeja, P. K. (2001) *Am. J. Physiol.* **281,** G144–G150
23. Parker, I., Callamaras, N., and Wier, W. G. (1997) *Cell Calcium* **21,** 441–452
24. Callamaras, N., and Parker, I. (1999) *Cell Calcium* **26,** 271–279
25. Janecki, A. J., Janecki, M., Akhter, S., and Donowitz, M. (2000) *J. Histochem. Cytochem.* **48,** 1479–1481
26. Sweet, D. H., Miller, D. S., and Pritchard, J. B. (2000) *Am. J. Physiol.* **279,** F826–F834
27. Matter, K., and Mellman, I. (1994) *Curr. Opin. Cell Biol.* **6,** 545–554
28. Caplan, M. J. (1997) *Am. J. Physiol.* **272,** F425–F429
29. Suzuki, T., Fujikura, K., Koyama, H., Matsuzaki, T., Takahashi, Y., and Takata, K. (2001) *Eur. J. Cell Biol.* **80,** 765–774
30. Sun, A.-Q., Arrese, M. A., Zeng, L., Swaby, I., Zhou, M. M., and Suchy, F. J. (2001) *J. Biol. Chem.* **276,** 6825–6833
31. Sirotnak, F. M., and Tolner, B. (1999) *Annu. Rev. Nutr.* **19,** 91–122
32. Ferguson, P. L., and Flintoff, W. F. (1999) *J. Biol. Chem.* **23,** 16269–16278
33. Oishi, K., Hirai, T., Gelb, B. D., and Diaz, G. A. (2001) *Mol. Genet. Metab.* **73,** 149–159
34. Parks, G. D., and Lamb, R. A. (1993) *J. Biol. Chem.* **268,** 19101–19109
35. Goswitz, V. C., and Brokker, R. J. (1995) *Protein Sci.* **4,** 534–537
36. Eudy, J. D., Spiegel, O., Barber, R. C., Wlodarczyk, B. J., Talbot, J., and Finnell, R. H. (2000) *Mol. Genet. Metab.* **71,** 581–590
37. Rajgopal, A., Edmondson, A., Goldman, D., and Zhao, R. (2001) *Biochim. Biophys. Acta* **1537,** 175–178
38. Scharfe, C., Hauschild, M., Klopstock, T., Janssen, A. J., Heidemann, P. H., Meitinger, T., and Jaksch, M. (2000) *J. Med. Genet.* **37,** 674–679
39. Trinczek, B., Ebneth, A., Mandelkow, E.-M., and Mandelkow, E. (1999) *J. Cell Sci.* **112,** 2355–2367
40. Fletcher, L. M., Welsh, G. I., Oatey, P. B., and Tavare, J. M. (2000) *Biochem. J.* **352,** 267–276
41. Hirokawa, N. (1998) *Science* **279,** 519–526